IEEE Access
Multidisciplinary | Rapid Review | Open Access Journal

Received 14 May 2024, accepted 7 June 2024, date of publication 11 June 2024, date of current version 9 July 2024.

Digital Object Identifier 10.1109/ACCESS.2024.3412956

RESEARCH ARTICLE

Research on GNSS-Assisted Low-Cost INS Combined Navigation Moving Base Initial Alignment Technique

MENGBO SUN[1], JIAN HUANG[1,2], PENGCHENG HU[1], XIAOHUI SONG[1], AND ZHU LI[1], (Member, IEEE)

[1]College of Geomatics and Geoinformation, Guilin University of Technology, Guilin 541004, China
[2]Guangxi Natural Resources Product Quality Inspection Center, Nanning 530200, China

Corresponding author: Jian Huang (2120201690@glut.edu.cn)

This work was supported by the National Natural Science Foundation of China under Grant 41864002.

ABSTRACT Aiming at the initial alignment problem of low-cost INS/GNSS in the case of moving base, this paper proposes a set of GNSS-assisted low-cost INS combined navigation initial alignment schemes, which is designed, optimized, and verified. Firstly, this paper analyses the impact of accelerometer zero bias on the accuracy of multi-vector construction and proposes an improved vector construction method, which approximates the suppression of the error caused by the accelerometer zero bias accumulating over time by vector subtraction instead of sliding window integration and also overcomes the impact of the OBA algorithm's computational increase and memory occupation caused by the fact that the sliding window integration needs to store and integrate the data in the window. Secondly, this paper also designs an improved Kalman filter model to reconstruct the state equation and measurement equation of the system, which can more accurately estimate the zero bias of the gyroscope online and compensate for the misalignment angle of the carrier system by using the velocity and position information of the GNSS, eliminating the influence of the zero bias of the gyroscope on the accuracy of the multi-vector, and improving the accuracy of the initial alignment of the moving base and the robustness of the algorithm. Finally, the algorithm proposed in this paper and other algorithms are compared and analyzed in simulation and vehicle test experiments. The simulation experiments verify the feasibility of the initial alignment method proposed in this paper; the vehicle test experiments use vector subtraction and sliding window integration to construct the multivector, and then estimate the zero bias of the gyroscope and compensate for the misalignment angle of the carrier system by using Kalman filtering model proposed in this paper and other Kalman filtering models, respectively. The measured results show that the proposed method has better alignment accuracy and algorithm robustness than the existing Optimization-based alignment and their improvement algorithms for the moving base of low-cost INS/GNSS combined navigation.

INDEX TERMS Low-cost SINS/GNSS, optimization-based alignment, Kalman filtering.

I. INTRODUCTION

The inertial navigation system is one of the important navigation technologies in the field of navigation, and initial alignment is a calibration work that must be carried out before the use of an inertial navigation system. The accuracy of initial alignment not only affects the accuracy of subsequent navigation but also affects the time for the whole combined navigation system to start. Therefore, accurate and efficient initial alignment has been regarded as one of the key technologies of inertial navigation systems [2], [4]. Depending on the motion state of the base (e.g., indoor test bed or carrier) connected to the inertial measurement unit, the alignment process of an inertial navigation system can be divided into

The associate editor coordinating the review of this manuscript and approving it for publication was Angelo Trotta.

two ways: static base alignment and moving base alignment. Dynamic pedestal alignment is performed in the motion state of the carrier body, and the process aims to ensure that the inertial navigation system can accurately acquire the initial attitude information [5], [6].

In the past decades, many researchers have thoroughly studied the initial alignment problem of the moving base and proposed many different algorithms. Some of the commonly used methods are the compass alignment method, geomagnetic survey alignment, GNSS velocity orientation, dual/multi-antenna GNSS attitude measurement, and multi-information combination estimation [1]

The compass alignment method consists of two steps, firstly horizontal alignment, which uses a gyroscope to measure the attitude of the device, and then azimuthal alignment, which aligns the initial position of the device according to the pointing of the compass. In 2019, Yu [7] proposed the use of forward and reverse navigation to solve the Jetlink compass full-cycle and half-cycle alignment method, which improves the real-time performance of the moving base alignment and the optimal configuration of the parameters. With the development of science and technology, the compass alignment gradually fades out of our vision. Geomagnetic measurement for azimuthal alignment is to determine the position information of the inertial guidance equipment by collecting the distribution characteristics of the earth's magnetic field, which requires the use of a magnetometer to collect geomagnetic information. In the process of use, the magnetometer needs to be calibrated and error corrected to ensure the accuracy of the measurement results.

In 2021, Gao [8] proposed a solution to solve the problem of real-time calibration of MEMS gyro degradation parameters, including the establishment of an equivalent linear model of performance degradation gyro, and proposed a recursive least squares parameter estimation method based on the geomagnetic information Gossypol effect model, as well as an adaptive EKF full attitude estimation algorithm based on the information of the geomagnetic/MEMS gyro/ballistic characteristics. These methods can estimate the attitude angle, angular velocity, angular acceleration, and other information of the carrier in real time, which has the advantages of good real-time performance and high estimation accuracy. However, the magnetometer is sensitive to metal and other items that can easily cause magnetic field changes, and the reliability is insufficient.

Shin and Sheimy [9] introduced the method of GNSS velocity orientation, after the completion of the polearm correction, the horizontal plane roll angle and pitch angle are almost zero, and the heading angle can be roughly estimated using the speed of GNSS as a way of substituting into the IMU to complete the initial work, but the GNSS velocity orientation exists a 180° heading angle error in the reversing, which brings some inconvenience to the practical application [10]. Dual/multiple antenna GNSS posing is a GPS interferometer that includes two antennas separated in distance, by measuring the carrier phase difference of multiple satellites on the two antennas, the baseline vectors composed of the two antennas can be solved. The three attitude angles of the carrier can then be measured from the three linearly independent interferometers. Dual/multi-antenna GNSS attitude measurement hardware is relatively costly and subject to multipath effects and carrier rigidity conditions and does not apply to low-cost INS.

The algorithm studied in this paper also belongs to the multi-information combination estimation, which uses optimal estimation theory (e.g., least squares, Kalman filter, gradient descent, etc.) and other sensors (e.g., GNSS receivers) to assist the INS in the initial alignment. The algorithm studied in this paper also belongs to the multi-information combination estimation. M. Wu and Y. Wu [11] first proposed a novel idea of Optimization-based alignment (OBA), which decomposes the required attitude matrix into two time-varying attitude matrices and one constant attitude matrix and uses the quaternion method to calculate the time-varying attitude matrix to determine the continuous attitude of the attitude.

In 2013, Wu and Pan [12], [13] proposed an OBA algorithm based on the velocity/position integral equation, which avoids the serious noise amplification effect caused by GNSS differentiation. However, the OBA algorithm does not consider the effects caused by IMU errors and directly uses IMU output data to participate in the calculation, and the uncompensated sensor errors will accumulate over time. Therefore, the OBA algorithm is not suitable for low-accuracy INS [14].In 2019, Xu [15] proposed a moving base alignment method for combined INS/GNSS systems based on position trajectories by reconstructing the vectors of the OBA algorithm. Since the algorithm does not need to use the GNSS velocity and constructing the vector based on the position trajectory can suppress the outlier interference contained in the GNSS position output, it extends the applicability and robustness of the OBA algorithm, but the algorithm still needs the GNSS to provide the initial velocity for the initialization of the alignment. In 2021, Yao [16] used vector subtraction to put in the algorithm of the literature [15], which makes the algorithm no longer need the GNSS initial velocity for initialization, expanding the applicability and avoiding the interference of initial velocity outliers. However, they did not consider the effect of IMU error accumulation over time, and GNSS has cm-level positioning accuracy and cm/s velocimetry accuracy when INS/GNSS combined navigation is carried out with GNSS defaulting to carrier-phase differential positioning mode. Therefore, this algorithm is more suitable for the case where INS with higher accuracy and auxiliary sensors cannot provide good information.

Huang [17] et al. combined the OBA algorithm with Kalman filtering to estimate the misalignment angle caused by gyroscope error using the odometer as an auxiliary sensor and fed the estimation results back to the OBA algorithm to improve the alignment accuracy. Although the effect of IMU error is considered in the algorithm, it is not estimated,

and the gyroscope error needs to be set manually based on experience. Chang [18] proposes to use the sliding window integral to suppress the accumulation of accelerometer error, to improve the alignment accuracy of the OBA algorithm. However, L. Chang did not consider the effect of gyroscope error, and the sliding window integration needs to strictly store and integrate the data in the window, which increases the computation amount of the OBA algorithm. To shorten the time of the initial alignment process, Chang [19], [20] established the Attitude Determination-based Initial Alignment (ADIA) vector observation construction based on the OBA method by reusing the measurement data from GNSS and IMU, and by using the concept of backward navigation. The backtracking integration procedure of ADIA, however, the backtracking integration method is essentially exhaustive, so it is not considered efficient and has limited efficiency in accelerating the initial alignment, although it can slightly improve the efficiency through some pruning operations, it is still a relatively inefficient algorithm, and it still does not take into account the effect of the gyroscope error on the accuracy of the OBA vectors.

To solve the effect of gyroscope errors on the OBA algorithm, Chang [21] proposed a linear indirect Kalman filtering model based on the OBA algorithm to estimate the constant zero bias of the gyroscope and compensate for the attitude errors in 2017. Lu [22] combined two methods, sliding window integration and indirect Kalman filtering, and using gradient descent to solve the multi-vector stance fixing in the projectile air alignment achieving better results. However, the indirect Kalman filtering model in literature [21] is an online estimation and compensation of the attitude error at the initial moment, rather than an online estimation and compensation of the attitude error at the current moment, and when it is applied in low-cost MEMS-IMUs, if the initial alignment time is a little long, it is impossible to estimate and compensate the attitude misalignment angle at the subsequent time, and when it encounters a large initial misalignment of the heading, it will destroy the small angle assumptions, leading to the case of initial alignment failure: while the gradient descent method has the disadvantages that it is only advantageous when the sample size is large enough and may find a solution that is not globally optimal. To enable the OBA algorithm to estimate and compensate the attitude error during the moving base alignment process, and to enable the OBA algorithm to be applied to low accuracy INS, Wang [23] et al. combined the Adaptive Unscented Kalman Filter (AUKF) with the OBA algorithm, and by combining the loaded system and the computed loaded system with the error equation modeling, a new Fast In-Motion Alignment (FIMA) algorithm for GNSS-assisted INS was proposed.

Liu [24] and Chen [25] combined the sliding window integration and FIMA methods to propose a Type-2 Fuzzy Adaptive Kalman Filter (T-2FAKF) algorithm and an Adaptive State Transformation Kalman Filter (ASTKF) algorithm, respectively, to make OBA The algorithm can suppress the accumulation of accelerometer errors and estimate the compensation attitude error online during the alignment process of low-cost INS moving base. However, there are some shortcomings in the system model of the FIMA algorithm, which may not be able to compensate for the attitude error well. In addition, many GNSS-assisted OBA algorithms for INS have been developed [26], [31]. However, most of these studies focus on high-level IMUs, and only a few studies focus on low-end MEMS-IMUs using the complex nonlinear Unscented Kalman Filter (UKF), and there are computational complexity issues in practical applications.

In this paper, for the GNSS-assisted low-cost INS combined navigation movable base initial alignment problem, we design a movable base initial alignment scheme applicable to low-cost INS/GNSS combined navigation system and verify the feasibility of the algorithm from the simulation experiments and vehicle measurement experiments, to provide some valuable references for the practical applications.

The article is structured as follows. In Section II, we introduce the theoretical basis and limitations of the OBA algorithm. We also present improvements to overcome its shortcomings. In Section III, we discuss the theoretical basis and limitations of the EKF and FIMA algorithms, and how the authors improved the Kalman filter algorithm. Sections IV and V describe simulation and vehicle experiments, respectively, to demonstrate the feasibility and effectiveness of the proposed algorithm. Finally, in Section VI, we provide some discussion and conclusions for the article.

II. OBA ALGORITHM AND ITS IMPROVEMENT

A. OBA ALGORITHM BASIS AND DEFICIENCIES

Combined navigation is a multi-coordinate system problem, and the commonly used coordinate systems covered in this paper are inertial coordinate system (i-system), geocentric geoid coordinate system (e-system), navigation coordinate system (n-system), and sensor coordinate system (b-system).

The OBA algorithm is derived from the inertial ground speed differential equation, M. Wu [11] et al. made a detailed derivation of this process, and this paper directly quotes the following formula:

$$\mathbf{C}_b^n(0)\boldsymbol{\alpha}_v = \boldsymbol{\beta}_v \tag{1}$$

Equation (1) is the velocity integral equation of the OBA algorithm, where:

$$\begin{aligned}\boldsymbol{\alpha}_v &\triangleq \int_0^t \mathbf{C}_{b(t)}^{b(0)} f^b dt \\ \boldsymbol{\beta}_v &\triangleq \mathbf{C}_{n(t)}^{n(0)}\mathbf{v}^n - \mathbf{v}^n(0) + \int_0^t \mathbf{C}_{n(t)}^{n(0)}\boldsymbol{\omega}_{ie}^n \times \mathbf{v}^n dt - \int_0^t \mathbf{C}_{n(t)}^{n(0)}\mathbf{g}^n dt\end{aligned} \tag{2}$$

In Eq. (1) and Eq. (2), $\mathbf{C}_{b(t)}^{b(0)}$ is the attitude change matrix of the b series at 0-t time. $\mathbf{C}_{n(t)}^{n(0)}$ is the N-series attitude change matrix at 0-t time; $\mathbf{C}_b^n(0)$ is the attitude matrix at time 0 of the initial alignment algorithm. $\mathbf{C}_{b(t)}^{b(0)}$, $\mathbf{C}_{n(t)}^{n(0)}$ are time-varying matrices, and $\mathbf{C}_b^n(0)$ is constant matrices. $\boldsymbol{\alpha}_v$ is the reference

vector, which can be calculated by integrating $\mathbf{C}_{b(t)}^{b(0)}$ and the specific force vector $\boldsymbol{f}^b$ measured by the accelerometer; $\boldsymbol{\beta}_v$ is the observation vector, which can be calculated from $\mathbf{C}_{n(t)}^{n(0)}$ and GPS output v^n and g^n integrals.

Theoretically, if there are two non-collinear vectors ($\boldsymbol{\alpha}_v$ and $\boldsymbol{\beta}_v$), the initial attitude matrix $\mathbf{C}_b^n(0)$ can be uniquely determined. Over time, $\boldsymbol{\alpha}_v$ and $\boldsymbol{\beta}_v$ form multiple sets of vectors, so the essence of the OBA algorithm is a multi-vector posing algorithm, that is, to seek the optimal solution of $\mathbf{C}_b^n(0)$.

However, the traditional OBA algorithm is calculated directly using the IMU output and cannot estimate and compensate, while the gyroscope bias, accelerometer bias, noise, etc. will cause the attitude error to diverge over time, so the traditional OBA algorithm is more suitable for high-precision SINS systems. This flaw is even more pronounced in the case of low-precision SINS systems. Next, this paper will improve the traditional OBA algorithm to suppress accelerometer bias.

B. VECTOR SUBTRACTION CONSTRUCTS α_v AND β_v

Accelerometer bias will cause the attitude error to diverge with time under the integration operation of obtaining information such as carrier velocity and position, so the accelerometer bias accumulation can be suppressed by shortening the integration interval. At the time t_k, the integral interval of the vector $\boldsymbol{\alpha}$ is constructed as two intervals $(0, t_{k-1})$ and (t_{k-1}, t_k), according to Eq. (2), the formula for calculating the vector $\boldsymbol{\alpha}$ at a time t_k can be written as:

$$\boldsymbol{\alpha}_v(t_k) = \int_0^{t_k} \mathbf{C}_{b(t)}^{b(0)} \boldsymbol{f}^b dt = \int_0^{t_{k-1}} \mathbf{C}_{b(t)}^{b(0)} \boldsymbol{f}^b dt + \int_{t_{k-1}}^{t_k} \mathbf{C}_{b(t)}^{b(0)} \boldsymbol{f}^b dt \tag{3}$$

The formula for calculating the vector $\boldsymbol{\alpha}$ at moment t_{k-1} can be written as:

$$\boldsymbol{\alpha}_v(t_{k-1}) = \int_0^{t_{k-1}} \mathbf{C}_{b(t)}^{b(0)} \boldsymbol{f}^b dt \tag{4}$$

To construct $\tilde{\boldsymbol{\alpha}}(t_k) = \boldsymbol{\alpha}(t_k) - \boldsymbol{\alpha}(t_{k-1})$, the formula for calculating the vector $\tilde{\boldsymbol{\alpha}}$ at time t_k can be written as:

$$\tilde{\boldsymbol{\alpha}}_v(t_k) = \boldsymbol{\alpha}_v(t_k) - \boldsymbol{\alpha}_v(t_{k-1}) = \int_{t_{k-1}}^{t_k} \mathbf{C}_{b(t)}^{b(0)} \boldsymbol{f}^b dt \tag{5}$$

Correspondingly, the formula for calculating the vector $\boldsymbol{\beta}$ at moment t_k can be written as:

$$\begin{aligned}\boldsymbol{\beta}_v(t_k) &= \mathbf{C}_{n(t_k)}^{n(0)} \mathbf{v}^n(t_k) - \mathbf{v}^n(0) + \int_0^{t_k} \mathbf{C}_{n(t)}^{n(0)} \boldsymbol{\omega}_{ie}^n \\ &\quad \times \mathbf{v}^n dt - \int_0^{t_k} \mathbf{C}_{n(t)}^{n(0)} \mathbf{g}^n dt \\ &= \mathbf{C}_{n(t_k)}^{n(0)} \mathbf{v}^n(t_k) - \mathbf{v}^n(0) + \int_0^{t_{k-1}} \mathbf{C}_{n(t)}^{n(0)} \boldsymbol{\omega}_{ie}^n \times \mathbf{v}^n dt \\ &\quad + \int_{t_{k-1}}^{t_k} \mathbf{C}_{n(t)}^{n(0)} \boldsymbol{\omega}_{ie}^n \times \mathbf{v}^n dt \\ &\quad - \int_0^{t_{k-1}} \mathbf{C}_{n(t)}^{n(0)} \mathbf{g}^n dt - \int_{t_{k-1}}^{t_k} \mathbf{C}_{n(t)}^{n(0)} \mathbf{g}^n dt \end{aligned} \tag{6}$$

The formula for calculating the vector $\boldsymbol{\beta}$ at moment t_{k-1} can be written as:

$$\begin{aligned}\boldsymbol{\beta}_v(t_{k-1}) &= \mathbf{C}_{n(t_{k-1})}^{n(0)} \mathbf{v}^n(t_{k-1}) - \mathbf{v}^n(0) \\ &\quad + \int_0^{t_{k-1}} \mathbf{C}_{n(t)}^{n(0)} \boldsymbol{\omega}_{ie}^n \times \mathbf{v}^n dt - \int_0^{t_{k-1}} \mathbf{C}_{n(t)}^{n(0)} \mathbf{g}^n dt \end{aligned} \tag{7}$$

To construct $\tilde{\boldsymbol{\beta}}(t_k) = \boldsymbol{\beta}(t_k) - \boldsymbol{\beta}(t_{k-1})$, the formula for calculating the vector $\tilde{\boldsymbol{\beta}}$ at moment t_k can be written as:

$$\begin{aligned}\tilde{\boldsymbol{\beta}}_v(t_k) &= \boldsymbol{\beta}_v(t_k) - \boldsymbol{\beta}_v(t_{k-1}) \\ &= \mathbf{C}_{n(t_k)}^{n(0)} \mathbf{v}^n(t_k) - \mathbf{C}_{n(t_{k-1})}^{n(0)} \mathbf{v}^n(t_{k-1}) \\ &\quad + \int_{t_{k-1}}^{t_k} \mathbf{C}_{n(t)}^{n(0)} \boldsymbol{\omega}_{ie}^n \times \mathbf{v}^n dt - \int_{t_{k-1}}^{t_k} \mathbf{C}_{n(t)}^{n(0)} \mathbf{g}^n dt \end{aligned} \tag{8}$$

Obviously, according to Eq. (1), we get:

$$\tilde{\boldsymbol{\beta}}_v(t_k) = \mathbf{C}_b^n(0) \tilde{\boldsymbol{\alpha}}_v(t_k) \tag{9}$$

Equations (5), (8), and (9) are the basic equations proposed in this paper to construct the vectors of the OBA algorithm by vector subtraction. In this method, the calculation integration interval is fixed at (t_{k-1}, t_k) and does not need to start from time 0, so the integration interval will not change with the alignment time, which can ensure that the accelerometer bias accumulation can be effectively suppressed during the entire alignment process. At the same time, the method does not store the integration results like the sliding window integration, and on the premise of ensuring accuracy, it also subtracts the amount of calculation and improves the alignment efficiency.

III. KALMAN FILTER SUPPRESSES GYROSCOPE ERROR ACCUMULATION

A. EKF ALGORITHM BASIS AND DEFICIENCIES

According to the above, the improved vector construction and calculation method can inhibit the accumulation of accelerometer bias. However, the gyroscope angular rate still needs to be integrated from time 0 to ensure the attitude calculation of the carrier. The gyro bias will inevitably seriously affect the accuracy of the vector with time integration, and then increase the attitude error. Therefore, based on the improved vector construction in 2.1, by combining with the GNSS navigation information, the indirect Kalman filter is used to identify the gyroscope bias and attitude error, and the attitude error is fed back to the construction process of multiple vectors, to correct the attitude matrix.

According to the rules of chain multiplication, there are:

$$\mathbf{C}_b^n = \mathbf{C}_{n'}^n \mathbf{C}_b^{n'} \tag{10}$$

When the misalignment angle under the n system is small, according to the equivalent rotation vector and direction cosine relationship, the approximation is:

$$\mathbf{C}_{n'}^n \approx I + (\boldsymbol{\phi}\times) \tag{11}$$

where $\boldsymbol{\phi}$ is the equivalent rotation vector and $\boldsymbol{\phi}\times$ is the antisymmetric matrix of $\boldsymbol{\phi}$.

Transpose Eq. (11) and bring Eq. (10) into:

$$\mathbf{C}_b^n = [I + (\boldsymbol{\phi}\times)]\,\mathbf{C}_b^{n'} \tag{12}$$

$\mathbf{C}_b^n$ in Eq. (12) is the error-free attitude matrix

Eq. (13) is the differential equation for solving A in the ideal state, but in practice, the quantities are calculated with error, expressed as Eq. (14).

$$\dot{\mathbf{C}}_b^n = \mathbf{C}_b^n(\boldsymbol{\omega}_{ib}^b\times) - (\boldsymbol{\omega}_{in}^n\times)\mathbf{C}_b^n \tag{13}$$

$$\dot{\mathbf{C}}_b^{n'} = \mathbf{C}_b^{n'}(\tilde{\boldsymbol{\omega}}_{ib}^b\times) - (\tilde{\boldsymbol{\omega}}_{in}^n\times)\mathbf{C}_b^{n'} \tag{14}$$

where:

$$\tilde{\boldsymbol{\omega}}_{ib}^b = \boldsymbol{\omega}_{ib}^b + \delta\boldsymbol{\omega}_{ib}^b \tag{15}$$

$$\tilde{\boldsymbol{\omega}}_{in}^n = \boldsymbol{\omega}_{in}^n + \delta\boldsymbol{\omega}_{in}^n \tag{16}$$

$\boldsymbol{\omega}_{ib}^b$ is the three-axis output of the gyroscope, $\boldsymbol{\omega}_{in}^n$ can be calculated by the position and speed of the GPS output, $\delta\boldsymbol{\omega}_{ib}^b$ is the measurement error of the gyroscope, and $\delta\boldsymbol{\omega}_{in}^n$ is the calculation error of the navigation system [21].

Differentiating both sides of Eq. (13) at the same time, i.e., there is:

$$-\left(\dot{\boldsymbol{\phi}}\times\right)\mathbf{C}_b^{n'} + (I + \boldsymbol{\phi}\times)\,\dot{\mathbf{C}}_b^{n'} = \mathbf{C}_b^n(\tilde{\boldsymbol{\omega}}_{ib}^b\times) - (\tilde{\boldsymbol{\omega}}_{in}^n\times)\mathbf{C}_b^n \tag{17}$$

Then bring Eq. (12), Eq. (13), Eq. (15) and Eq. (16) into Eq. (17) and multiply $C_{n'}^b$ on both sides of the equation and simplify it to obtain:

$$\begin{aligned}(\dot{\boldsymbol{\phi}}\times) = &\left[(\boldsymbol{\phi}\times)(\boldsymbol{\omega}_{in}^n\times) - (\boldsymbol{\omega}_{in}^n\times)(\boldsymbol{\phi}\times)\right] \\ &+ (\delta\boldsymbol{\omega}_{in}^n\times) - \mathbf{C}_b^{n'}(\delta\boldsymbol{\omega}_{ib}^b\times)\mathbf{C}_{n'}^b\end{aligned} \tag{18}$$

The result is:

$$\dot{\boldsymbol{\phi}} = \boldsymbol{\phi}\times\boldsymbol{\omega}_{in}^n + \delta\boldsymbol{\omega}_{in}^n - \delta\boldsymbol{\omega}_{ib}^n \tag{19}$$

where the angular velocity denoted by $\boldsymbol{\omega}_{in}^n$ is caused by the Earth's rotation in inertial space, and the value is small and negligible for inertial devices; The measurement error represented is caused by the gyroscope constant bias $\boldsymbol{\varepsilon}^b$, which can be approximated as:

$$\delta\boldsymbol{\omega}_{ib}^n \approx \boldsymbol{\varepsilon}^n = \boldsymbol{C}_b^n\boldsymbol{\varepsilon}^b \tag{20}$$

Bringing Eq. (19) into Eq. (20) yields:

$$\dot{\boldsymbol{\phi}} \approx -\boldsymbol{C}_b^{n'}\boldsymbol{\varepsilon}^b \tag{21}$$

Eq. (21) is the equation of state of the system when the extended Kalman filter is applied to the OBA algorithm [21].

According to the multiplication rules, there are:

$$\mathbf{C}_{b(0)}^{n(0)} = \mathbf{C}_{n'(0)}^{n(0)}\mathbf{C}_{b(0)}^{n'(0)} = (\boldsymbol{I} + \boldsymbol{\phi}'\times)\mathbf{C}_{b(0)}^{n'(0)} \tag{22}$$

Eq. (9) can be written as:

$$\tilde{\boldsymbol{\beta}}_v = (\boldsymbol{I} + \boldsymbol{\phi}'\times)\mathbf{C}_{b(0)}^{n'(0)}\tilde{\boldsymbol{\alpha}}_v \tag{23}$$

where $\boldsymbol{\phi}'$ is the equivalent rotation vector from n to n' at the initial moment.

For Eq. (23), the measurement equation for the extended Kalman filter applied to the OBA algorithm is simplified and sorted out, as follows:

$$\mathbf{C}_b^{n'}(0)\tilde{\boldsymbol{\alpha}}_v - \tilde{\boldsymbol{\beta}}_v = \left((\mathbf{C}_b^{n'}(0)\tilde{\boldsymbol{\alpha}}_v)\times\right)\boldsymbol{\phi}' \tag{24}$$

Define the amount of system state $\boldsymbol{X}_{k+1} = \left[\left(\boldsymbol{\phi}'_{k+1}\right)^T \left(\boldsymbol{\varepsilon}'_{k+1}\right)^T\right]^T$ at time t_{k+1}, then the system state space model is:

$$\begin{cases}\boldsymbol{X}_{k+1} = \boldsymbol{\Phi}_{k+1/k}\boldsymbol{X}_k + \boldsymbol{\Gamma}_k\boldsymbol{W}_k \\ \boldsymbol{Z}_{k+1} = \boldsymbol{H}_{k+1}\boldsymbol{X}_{k+1} + \boldsymbol{V}_{k+1}\end{cases} \tag{25}$$

Thereinto:

$$\boldsymbol{\Phi}_{k+1/k} = \begin{bmatrix}\boldsymbol{I}_{3\times3} & -\mathbf{C}_b^{n'}(0)T \\ \mathbf{0}_{3\times3} & \boldsymbol{I}_{3\times3}\end{bmatrix} \tag{26}$$

$$\boldsymbol{H}_{k+1} = \begin{bmatrix}\mathbf{C}_{b(0)}^{n'(0)}\,(\tilde{\boldsymbol{\alpha}}_v\times)\ \mathbf{0}_{3\times3}\end{bmatrix} \tag{27}$$

$$\boldsymbol{Z}_{k+1} = \mathbf{C}_b^{n'}(0)\tilde{\boldsymbol{\alpha}}_v - \tilde{\boldsymbol{\beta}}_v \tag{28}$$

where $\boldsymbol{\Phi}_{k+1/k}$ is the transition matrix of the system state from time t_k to time t_{k+1};$\boldsymbol{\Gamma}_k$ is the system noise driving matrix; $\boldsymbol{W}_k$ is the white noise matrix of the system; $\boldsymbol{Z}_{k+1}$ is the measurement vector at the time t_{k+1}; $\boldsymbol{H}_{k+1}$ is the parameter matrix of the measurement system; $\boldsymbol{V}_{k+1}$ is the measurement white noise matrix. $\boldsymbol{W}_k$ and $\boldsymbol{V}_k$ are Gaussian white noise processes that are uncorrelated and both have zero mean [32].

Using equation (25)-(28), the gyroscope bias $\boldsymbol{\varepsilon}^b$ can be estimated online, and the initial attitude error $\boldsymbol{\phi}'$ estimation result of the Kalman filter can be fed back to the multi-vector construction process to suppress the gyroscope error accumulation.

However, since $\boldsymbol{\phi}'$ is the equivalent rotation vector from n to n' at the initial time, the extended Kalman filter model is to estimate and compensate for the attitude error at the initial moment, rather than the online estimation and compensation of the attitude error at the current moment. Secondly, since Eq. (11) is established under the assumption that $\boldsymbol{\phi}'$ is a small angle, the extended Kalman filter will destroy this assumption when it encounters a large initial heading misalignment (the OBA algorithm does not converge the heading misalignment angle to a small angle in a short time), failing the initial alignment. Therefore, the extended Kalman filter model is suitable for cases where the initial alignment time is not long (e.g., within a few seconds), because the heading misalignment angle after the initial alignment will converge to a small angle, and the assumption that $\boldsymbol{\phi}'$ is a small angle is valid, and because the time is short, the gyroscope does not accumulate too much error over time.

B. FIMA ALGORITHM BASIS AND DEFICIENCIES β_v

The attitude update matrix $\boldsymbol{C}_{b(t_{k+1})}^{b(0)}$ of the b system at zero time is calculated using the angular increment output by the gyroscope, but due to the existence of the gyroscope error, the angular increment $\Delta\boldsymbol{\theta}$ of the gyroscope output contains

the error, so the calculated $\boldsymbol{C}_{b(t_{k+1})}^{b(0)}$ also has an error, and the $\boldsymbol{C}_{b(t_{k+1})}^{b(0)}$ with the error is recorded as $\boldsymbol{C}_{b'(t_{k+1})}^{b(0)}$, according to the law of chain multiplication of the strap-down inertial attitude update matrix, the relationship between $\boldsymbol{C}_{b(t_{k+1})}^{b(0)}$ and $\boldsymbol{C}_{b'(t_{k+1})}^{b(0)}$ can be expressed as:

$$\boldsymbol{C}_{b(t_{k+1})}^{b(0)} = \boldsymbol{C}_{b'(t_{k+1})}^{b(0)} \boldsymbol{C}_{b(t_{k+1})}^{b'(t_{k+1})} \tag{29}$$

Bearing in mind that the calculated b system containing the gyroscope error is b', then the equivalent rotation vector between the ideally error-free b system and the calculated b' system containing the error is $\boldsymbol{\phi}_{bb'}$. In the short period of time when the alignment starts and the $\boldsymbol{C}_{b'(t_{k+1})}^{b(0)}$ feedback correction has not been carried out, the gyroscope zero bias accumulates a small error with time integration, and the misalignment angle caused by it is not large, and then the algorithm has been feeding back and correcting $\boldsymbol{C}_{b'(t_{k+1})}^{b(0)}$, so that $\boldsymbol{\phi}_{bb'}$ is always a small quantity, so the matrix $\boldsymbol{C}_{b(t_{k+1})}^{b'(t_{k+1})}$ can be approximated as:

$$\boldsymbol{C}_{b(t_{k+1})}^{b'(t_{k+1})} = \boldsymbol{I} - \left(\boldsymbol{\phi}_{bb'}\times\right) \tag{30}$$

Bring Eq. (30) into Eq. (29) to get

$$\boldsymbol{C}_{b(t_{k+1})}^{b(0)} = \boldsymbol{C}_{b'(t_{k+1})}^{b(0)} (\boldsymbol{I} - \boldsymbol{\phi}_{bb'}\times) \tag{31}$$

Deriving both sides of Eq. (31) at the same time yields:

$$\dot{\boldsymbol{C}}_{b(t_{k+1})}^{b(0)} = \dot{\boldsymbol{C}}_{b'(t_{k+1})}^{b(0)} (\boldsymbol{I} - \boldsymbol{\phi}_{bb'}\times) - \boldsymbol{C}_{b'(t_{k+1})}^{b(0)} \dot{\boldsymbol{\phi}}_{bb'}\times \tag{32}$$

Thereinto:

$$\dot{\boldsymbol{C}}_{b(t_{k+1})}^{b(0)} = \boldsymbol{C}_{b(t_{k+1})}^{b(0)} \left(\boldsymbol{\omega}_{ib}^{b}\times\right) = \boldsymbol{C}_{b(t_{k+1})}^{b(0)} \left(\left(\tilde{\boldsymbol{\omega}}_{ib}^{b}\times\right) - \left(\delta\tilde{\boldsymbol{\omega}}_{ib}^{b}\times\right)\right) \tag{33}$$

where $\tilde{\boldsymbol{\omega}}_{ib}^{b}$ is the angular rate of the gyroscope's output; $\delta\tilde{\boldsymbol{\omega}}_{ib}^{b}$ is the error of the angular rate output by the gyroscope, and the two satisfy the following relation:

$$\boldsymbol{\omega}_{ib}^{b} = \tilde{\boldsymbol{\omega}}_{ib}^{b} + \delta\boldsymbol{\omega}_{ib}^{b} \tag{34}$$

$$\delta\boldsymbol{\omega}_{ib}^{b} = \boldsymbol{\varepsilon}^{b} + \boldsymbol{w}_{g} \tag{35}$$

where $\boldsymbol{\omega}_{ib}^{b}$ is the theoretical error-free angular rate of gyroscope output; $\boldsymbol{\varepsilon}^{b}$is the gyroscope constant drift ($\dot{\boldsymbol{\varepsilon}}^{b} = 0_{3\times1}$); $\boldsymbol{w}_{g}$ is the measured white noise of the gyroscope.

Bringing Eq. (29), Eq. (30), Eq. (31), Eq. (33), and Eq. (34) into Eq. (32) yields:

$$\begin{aligned}&\boldsymbol{C}_{b'(t_{k+1})}^{b(0)} (\boldsymbol{I} - \boldsymbol{\phi}_{bb'}\times) \left[\left(\tilde{\boldsymbol{\omega}}_{ib}^{b} + \delta\boldsymbol{\omega}_{ib}^{b}\right)\times\right] \\ &\quad = \boldsymbol{C}_{b'(t_{k+1})}^{b(0)} \left(\tilde{\boldsymbol{\omega}}_{ib}^{b}\times\right) (\boldsymbol{I} - \boldsymbol{\phi}_{bb'}\times) - \boldsymbol{C}_{b'(t_{k+1})}^{b(0)} \dot{\boldsymbol{\phi}}_{bb'}\times\end{aligned} \tag{36}$$

Multiplication $\boldsymbol{C}_{b(0)}^{b'(t_{k+1})}$ on both sides of the equation and collation yields:

$$\begin{aligned}&\left(\tilde{\boldsymbol{\omega}}_{ib}^{b}\times\right) + \left(\delta\boldsymbol{\omega}_{ib}^{b}\times\right) - \left(\boldsymbol{\phi}_{bb'}\times\right) \left(\tilde{\boldsymbol{\omega}}_{ib}^{b}\times\right) - \left(\boldsymbol{\phi}_{bb'}\times\right) \left(\delta\boldsymbol{\omega}_{ib}^{b}\times\right) \\ &= \left(\tilde{\boldsymbol{\omega}}_{ib}^{b}\times\right) - \left(\tilde{\boldsymbol{\omega}}_{ib}^{b}\times\right) \left(\boldsymbol{\phi}_{bb'}\times\right) - \dot{\boldsymbol{\phi}}_{bb'}\times\end{aligned} \tag{37}$$

For Eq. (37), we apply Eq.
$(\boldsymbol{A}_1\times)(\boldsymbol{A}_2\times) - (\boldsymbol{A}_2\times)(\boldsymbol{A}_1\times) = [(\boldsymbol{A}_1 \times \boldsymbol{A}_2)\times]$and ignore the second-order decimals to obtain:

$$\left(\dot{\boldsymbol{\phi}}_{bb'}\times\right) = \left[\left(\boldsymbol{\phi}_{bb'} \times \tilde{\boldsymbol{\omega}}_{ib}^{b}\right)\times\right] - \delta\boldsymbol{\omega}_{ib}^{b}\times \tag{38}$$

Namely:

$$\begin{aligned}\dot{\boldsymbol{\phi}}_{bb'}\times &= -\tilde{\boldsymbol{\omega}}_{ib}^{b} \times \boldsymbol{\phi}_{bb'} - \delta\boldsymbol{\omega}_{ib}^{b}\times \\ &= -\tilde{\boldsymbol{\omega}}_{ib}^{b} \times \boldsymbol{\phi}_{bb'} - \boldsymbol{\varepsilon}^{b} - \boldsymbol{w}_{g}\end{aligned} \tag{39}$$

Eq. (40) is the differential equation between the b system and the b' system, which reflects the influence of gyroscope error on the attitude estimation accuracy of the strap-down inertial navigation system, and the error modeling of the strap-down inertial navigation system can be carried out through Eq. (39), to estimate and compensate the attitude misalignment angle of the strap-down inertial navigation system, and improve the alignment accuracy and application range of the OBA algorithm.

According to Eq. (40), the equivalent rotation vector $\boldsymbol{\phi}_{bb'}$ and the gyroscope constant drift $\boldsymbol{\varepsilon}^{b}$ are selected as the state quantity $\boldsymbol{X}$ of the FIMA algorithm, i.e.,

$$\boldsymbol{X} = \left[\left(\boldsymbol{\phi}_{bb'}\right)^{T} \left(\boldsymbol{\varepsilon}^{b}\right)^{T}\right]^{T} \tag{40}$$

Eq. (5), (8), and (9) at time t_{k+1} can be expressed as:

$$\hat{\boldsymbol{\alpha}}_{v}\left(t_{k+1}\right) \triangleq \boldsymbol{C}_{b(t_k)}^{b(0)} \boldsymbol{\alpha}_{t_a}^{t_{a+1}} \tag{41}$$

$$\begin{aligned}\hat{\boldsymbol{\beta}}_{v}\left(t_{k+1}\right) \triangleq\ & \boldsymbol{C}_{n(t_{k+1})}^{n(0)} \boldsymbol{v}^{n}\left(t_{k+1}\right) - \boldsymbol{C}_{n(t_k)}^{n(0)} \boldsymbol{v}^{n}\left(t_k\right) \\ &+ \boldsymbol{C}_{n(t_k)}^{n(0)} \boldsymbol{\beta}_{t_a}^{t_{a+1}}\end{aligned} \tag{42}$$

$$\boldsymbol{C}_{b}^{n}(0)\, \hat{\boldsymbol{\alpha}}_{v}\left(t_{k+1}\right) = \hat{\boldsymbol{\beta}}_{v}\left(t_{k+1}\right) \tag{43}$$

For Eq. (41), we use the matrix multiplication chain rule:

$$\begin{aligned}\hat{\boldsymbol{\alpha}}_{v}\left(t_{k+1}\right) &\triangleq \boldsymbol{C}_{b(t_k)}^{b(0)} \boldsymbol{\alpha}_{t_a}^{t_{a+1}} \\ &= \boldsymbol{C}_{b'(t_{k+1})}^{b(0)} \boldsymbol{C}_{b(t_{k+1})}^{b'(t_{k+1})} \boldsymbol{C}_{b(t_k)}^{b(t_{k+1})} \boldsymbol{\alpha}_{t_a}^{t_{a+1}} \\ &= \boldsymbol{C}_{b'(t_{k+1})}^{b(0)} \left(\boldsymbol{I} - \boldsymbol{\phi}_{bb'}\times\right) \left(\boldsymbol{C}_{b(t_{k+1})}^{b(0)}\right)^{T} \boldsymbol{C}_{b(t_k)}^{b(0)} \boldsymbol{\alpha}_{t_a}^{t_{a+1}}\end{aligned} \tag{44}$$

Substituting Eq. (44) into Eq. (43) yields:

$$\begin{aligned}\hat{\boldsymbol{\beta}}_{v}\left(t_{k+1}\right) &= \boldsymbol{C}_{b}^{n}(0)\, \hat{\boldsymbol{\alpha}}_{v}\left(t_{k+1}\right) \\ &= \boldsymbol{C}_{b}^{n}(0)\, \boldsymbol{C}_{b'(t_{k+1})}^{b(0)} \left(\boldsymbol{I} - \boldsymbol{\phi}_{bb'}\times\right) \\ &\quad \left(\boldsymbol{C}_{b(t_{k+1})}^{b(0)}\right)^{T} \boldsymbol{C}_{b(t_k)}^{b(0)} \boldsymbol{\alpha}_{t_a}^{t_{a+1}} \\ &= \boldsymbol{C}_{b}^{n}(0)\, \boldsymbol{C}_{b'(t_{k+1})}^{b(0)} \left(\boldsymbol{C}_{b(t_{k+1})}^{b(0)}\right)^{T} \boldsymbol{C}_{b(t_k)}^{b(0)} \boldsymbol{\alpha}_{t_a}^{t_{a+1}} \\ &\quad + \boldsymbol{C}_{b}^{n}(0)\, \boldsymbol{C}_{b'(t_{k+1})}^{b(0)} \left[\left(\left(\boldsymbol{C}_{b(t_{k+1})}^{b(0)}\right)^{T} \boldsymbol{C}_{b(t_k)}^{b(0)} \boldsymbol{\alpha}_{t_a}^{t_{a+1}}\right)\right] \\ &\quad \boldsymbol{\phi}_{bb'}\times\end{aligned} \tag{45}$$

Shift Eq. (45):

$$\hat{\boldsymbol{\beta}}_v(t_{k+1}) - \boldsymbol{C}_b^n(0)\boldsymbol{C}_{b'(t_{k+1})}^{b(0)}\left(\boldsymbol{C}_{b(t_{k+1})}^{b(0)}\right)^T\boldsymbol{C}_{b(t_k)}^{b(0)}\boldsymbol{\alpha}_{t_a}^{t_{a+1}} = \boldsymbol{C}_b^n(0)\boldsymbol{C}_{b'(t_{k+1})}^{b(0)}\left[\left(\left(\boldsymbol{C}_{b(t_{k+1})}^{b(0)}\right)^T\boldsymbol{C}_{b(t_k)}^{b(0)}\boldsymbol{\alpha}_{t_a}^{t_{a+1}}\right)\right]\boldsymbol{\phi}_{bb'}\times \tag{46}$$

The system state space model of the FIMA algorithm is as follows:

$$\begin{cases}\boldsymbol{X}_{k+1} = \boldsymbol{\Phi}_{k+1/k}\boldsymbol{X}_k + \boldsymbol{\Gamma}_k\boldsymbol{W}_k\\ \boldsymbol{Z}_{k+1} = \boldsymbol{H}_{k+1}\boldsymbol{X}_{k+1} + \boldsymbol{V}_{k+1}\end{cases} \tag{47}$$

Thereinto:

$$\boldsymbol{\Phi}_{k+1/k} = \begin{bmatrix} -\left(\tilde{\boldsymbol{\omega}}_{ib}^b\times\right) + \boldsymbol{I}_{3\times3} & \boldsymbol{I}_{3\times3}\\ \boldsymbol{0}_{3\times3} & \boldsymbol{I}_{3\times3}\end{bmatrix} \tag{48}$$

$$\boldsymbol{H}_{k+1} = \left[\boldsymbol{C}_b^n(0)\boldsymbol{C}_{b'(t_{k+1})}^{b(0)}\left[\left(\left(\boldsymbol{C}_{b(t_{k+1})}^{b(0)}\right)^T\boldsymbol{C}_{b(t_k)}^{b(0)}\boldsymbol{\alpha}_{t_a}^{t_{a+1}}\right)\times\right]\boldsymbol{0}_{3\times3}\right] \tag{49}$$

$$\boldsymbol{Z}_{k+1} = \hat{\boldsymbol{\beta}}_v(t_{k+1}) - \boldsymbol{C}_b^n(0)\boldsymbol{C}_{b'(t_{k+1})}^{b(0)}\left(\boldsymbol{C}_{b(t_{k+1})}^{b(0)}\right)^T\boldsymbol{C}_{b(t_k)}^{b(0)}\boldsymbol{\alpha}_{t_a}^{t_{a+1}} \tag{50}$$

Using equation (48)-(50), the gyroscope bias $\boldsymbol{\varepsilon}^b$ can be estimated online, and the attitude error $\boldsymbol{\phi}_{bb'}$ result of the current moment estimated by the Kalman filter can be fed back to the multi-vector construction process to suppress the gyroscope error accumulation.

Observation Eq. (44) shows that the attitude of t_{k+1} at the current moment has not been corrected, but it contains the relevant attitude matrix $\boldsymbol{C}_{b(t_{k+1})}^{b(0)}$ of the current moment t_{k+1}, but in practice we obtain $\boldsymbol{C}_{b'(t_{k+1})}^{b(0)}$ with gyroscope error, in other words, the attitude matrix $\boldsymbol{C}_{b(t_{k+1})}^{b(0)}$ of the FIMA algorithm does not consider the influence of gyroscope error, and may not be able to compensate for the attitude error well.

C. RECONSTRUCT THE FILTER MODEL TO COMPENSATE FOR THE ATTITUDE ERROR

Because the extended Kalman filter needs to be assumed that $\boldsymbol{\phi}'$ is a small angle to be established, it will cause the system to diverge in the face of a large heading misalignment angle, and the matrix $\boldsymbol{C}_{b(t_{k+1})}^{b(0)}$ of the FIMA algorithm does not consider the influence of gyroscope error, which may not be able to compensate for the attitude error well, and both methods have certain shortcomings and defects. Therefore, based on the improvement of the vector construction vector using the vector subtraction method above, a new Kalman filter model is designed, which uses GNSS velocity and position information to more accurately estimate the gyroscope's bias and compensate for the load system misalignment angle, which eliminates the influence of gyroscope bias on the accuracy of multiple vectors, and improves the accuracy and robustness of the initial alignment of the moving base.

According to Eq. (39), the equivalent rotation vector $\boldsymbol{\phi}_{bb'}$ at time t_k and the gyroscope constant drift $\boldsymbol{\varepsilon}^b$ are selected as the state quantities $\boldsymbol{X}$ of the new Kalman filter model, i.e.,

$$\boldsymbol{X} = \left[\left(\boldsymbol{\phi}_{bb'}\right)^T\left(\boldsymbol{\varepsilon}^b\right)^T\right]^T \tag{51}$$

Use vector subtraction to construct the OBA algorithm vector at moment t_{k+1}:

$$\hat{\boldsymbol{\alpha}}_v(t_{k+1}) \triangleq \boldsymbol{C}_{b(t_k)}^{b(0)}\boldsymbol{\alpha}_{t_a}^{t_{a+1}} \tag{52}$$

$$\hat{\boldsymbol{\beta}}_v(t_{k+1}) \triangleq \boldsymbol{C}_{n(t_{k+1})}^{n(0)}\boldsymbol{v}^n(t_{k+1}) - \boldsymbol{C}_{n(t_k)}^{n(0)}\boldsymbol{v}^n(t_k) + \boldsymbol{C}_{n(t_k)}^{n(0)}\boldsymbol{\beta}_{t_a}^{t_{a+1}} \tag{53}$$

$$\boldsymbol{C}_b^n(0)\hat{\boldsymbol{\alpha}}_v(t_{k+1}) = \hat{\boldsymbol{\beta}}_v(t_{k+1}) \tag{54}$$

Equation (52) uses the matrix multiplication chain rule:

$$\begin{aligned}\hat{\boldsymbol{\alpha}}_v &\triangleq (t_{k+1})\boldsymbol{C}_{b(t_k)}^{b(0)}\boldsymbol{\alpha}_{t_a}^{t_{a+1}}\\ &= \boldsymbol{C}_{b'(t_k)}^{b(0)}\boldsymbol{C}_{b(t_k)}^{b'(t_k)}\boldsymbol{\alpha}_{t_a}^{t_{a+1}}\\ &= \boldsymbol{C}_{b'(t_k)}^{b(0)}\left(\boldsymbol{I} - \boldsymbol{\phi}_{bb'}\times\right)\boldsymbol{\alpha}_{t_a}^{t_{a+1}}\end{aligned} \tag{55}$$

Substituting Eq. (55) into Eq. (54) yields:

$$\begin{aligned}&\hat{\boldsymbol{\beta}}_v(t_{k+1})\\ &= \boldsymbol{C}_b^n(0)\hat{\boldsymbol{\alpha}}_v(t_{k+1})\\ &= \boldsymbol{C}_b^n(0)\boldsymbol{C}_{b'(t_k)}^{b(0)}\left(\boldsymbol{I} - \boldsymbol{\phi}_{bb'}\times\right)\boldsymbol{\alpha}_{t_a}^{t_{a+1}}\\ &= \boldsymbol{C}_b^n(0)\boldsymbol{C}_{b'(t_k)}^{b(0)}\boldsymbol{\alpha}_{t_a}^{t_{a+1}} + \boldsymbol{C}_b^n(0)\boldsymbol{C}_{b'(t_k)}^{b(0)}\left(\boldsymbol{\alpha}_{t_a}^{t_{a+1}}\times\right)\boldsymbol{\phi}_{bb'}\end{aligned} \tag{56}$$

Move Eq. (56):

$$\begin{aligned}&\hat{\boldsymbol{\beta}}_v(t_{k+1}) - \boldsymbol{C}_b^n(0)\boldsymbol{C}_{b'(t_k)}^{b(0)}\boldsymbol{\alpha}_{t_a}^{t_{a+1}}\\ &\quad= \boldsymbol{C}_b^n(0)\boldsymbol{C}_{b'(t_k)}^{b(0)}\left(\boldsymbol{\alpha}_{t_a}^{t_{a+1}}\times\right)\boldsymbol{\phi}_{bb'}\end{aligned} \tag{57}$$

The system state space model of the Kalman filter algorithm designed in this paper is as follows:

$$\begin{cases}\boldsymbol{X}_{k+1} = \boldsymbol{\Phi}_{k+1/k}\boldsymbol{X}_k + \boldsymbol{\Gamma}_k\boldsymbol{W}_k\\ \boldsymbol{Z}_{k+1} = \boldsymbol{H}_{k+1}\boldsymbol{X}_{k+1} + \boldsymbol{V}_{k+1}\end{cases} \tag{58}$$

Thereinto:

$$\boldsymbol{\Phi}_{k+1/k} = \begin{bmatrix} -\left(\tilde{\boldsymbol{\omega}}_{ib}^b\times\right)T + I_{3\times3} & I_{3\times3}\\ 0_{3\times3} & I_{3\times3}\end{bmatrix} \tag{59}$$

$$\boldsymbol{H}_{k+1} = \left[\boldsymbol{C}_b^n(0)\boldsymbol{C}_{b'(t_k)}^{b(0)}\left(\boldsymbol{\alpha}_{t_a}^{t_{a+1}}\times\right)\boldsymbol{0}_{3\times3}\right] \tag{60}$$

$$\boldsymbol{Z}_{k+1} = \hat{\boldsymbol{\beta}}_v(t_{k+1}) - \boldsymbol{C}_b^n(0)\boldsymbol{C}_{b'(t_k)}^{b(0)}\boldsymbol{\alpha}_{t_a}^{t_{a+1}} \tag{61}$$

Eq. (58)-(61) is the new Kalman filter model designed in this paper. Comparing Eq. (56) and Eq. (45), it can be found that the filter model proposed in this paper uses the attitude matrix $\boldsymbol{C}_{b'(t_k)}^{b(0)}$ at the current time t_k to construct the filter model, and $\boldsymbol{C}_{b'(t_k)}^{b(0)}$ is the attitude matrix considering the gyroscope error, so the proposed filter model can estimate and compensate for the attitude error caused by the gyroscope better than the FIMA algorithm and feed back the results into the

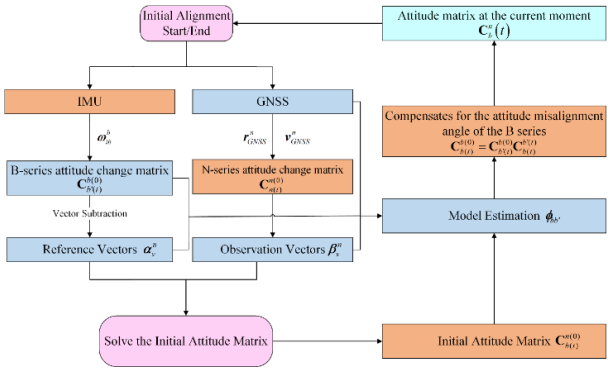

FIGURE 1. Flow chart of the proposed algorithm.

construction of multiple vectors. In this section, a new type of Kalman filter model is deduced in detail, which neither has the defect that the extended Kalman filter will destroy the small angle assumption, nor does the FIMA algorithm ignore the gyroscope error matrix $\boldsymbol{C}_{b(t)}^{b(0)}$, and by using the GNSS velocity and position information to more accurately estimate the gyroscope bias and compensate for the load system misalignment angle, the influence of gyroscope bias on the accuracy of multiple vectors is eliminated and theoretically provides a reference method for the initial alignment of the GNSS-assisted low-cost INS integrated navigation moving base.

IV. SIMULATION EXPERIMENTS

A. SIMULATION ENVIRONMENT SETTINGS

In order to verify the feasibility of the above algorithms, simulation experiments are used to evaluate the feasibility of the above algorithms. The simultaneous output of MIMU and high-precision GPS is set to facilitate the comparison of the value of the algorithm solution results in this paper.

The simulation experiment scenario is an ordinary vehicle motion scenario, the simulation parameter settings are shown in Table 1, the initial state setting of SINS is shown in Table 2, and the carrier motion state is shown in Figure 2-4, including the reference attitude, speed and trajectory of the carrier movement, and the motion process includes acceleration, deceleration, right turn, left turn, climbing, and uniform linear motion with a duration of 600 s.

B. SIMULATION RESULTS

The vector subtraction method and sliding window integration are used to construct the vectors, and then OBA, EKF, and the improved algorithm proposed in this paper are used to filter estimation and compensate for the attitude error, and the obtained results are compared and analyzed. VS-OBA is the OBA algorithm constructed by vector subtraction, SWI-EKF, and VS-EKF are the EKF algorithms constructed by sliding window integration and vector subtraction, respectively, Ref. is the reference value of high-precision instrument output, and PROPOSED is the improved algorithm proposed in this paper.

TABLE 1. Simulated IMU parameters.

Parameter	Specification
Gyro In-run Bias Stability	$10\ ^{\circ}/h$
Gyro Angle Random Walk	$0.1\ ^{\circ}/\sqrt{h}$
Acc. In-run Bias Stability	10 ug
Acc. Velocity Random Walk	$70m/s/\sqrt{h}$
IMU Refresh Rate	10 HZ
GPS Refresh Rate	10 Hz

TABLE 2. Simulated IMU parameters.

Parameter	Specification
Initial Latitude and Longitude Height	$[0 \quad 0 \quad 0]_{\circ}$
Initial Posture Angle	$[1 \quad -1 \quad 171]_{\circ}$
Initial Velocity	$[0 \quad 0 \quad 0]$ m/s

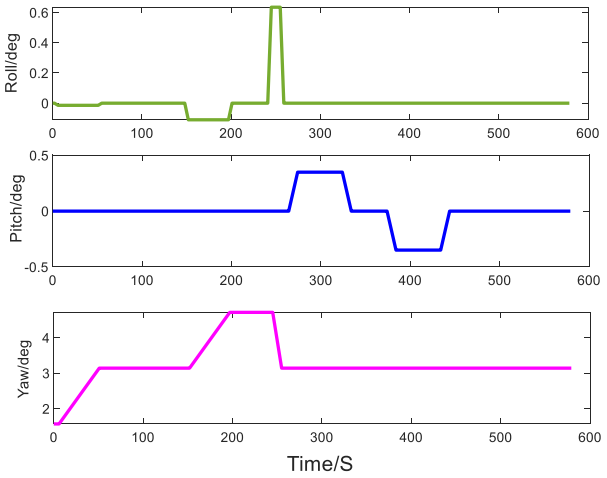

FIGURE 2. Reference posture.

Due to the serious divergence of the estimation results of the attitude angle of the SWI-EKF algorithm, the calculation results of 6-13 seconds are intercepted for comparison. As can be seen from Figure 5, the three attitude angles of the EKF filter compensation will show a tendency of divergence or fluctuation regardless of whether the sliding window integration or vector subtraction is used to construct the vector, because the heading misalignment angle in the initial misalignment angle set by the simulation is 171°, which destroys the small angle assumption of the extended

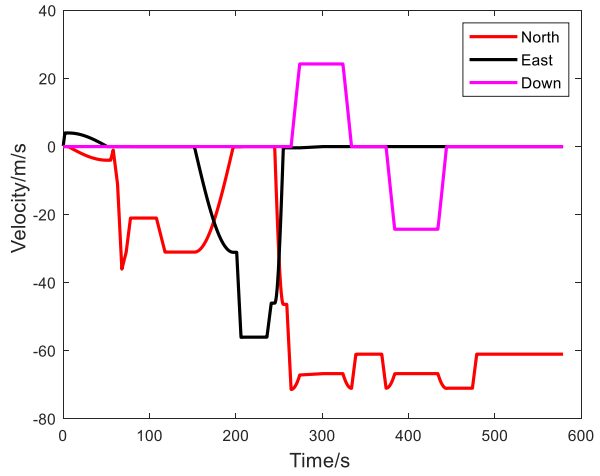

FIGURE 3. Reference speed.

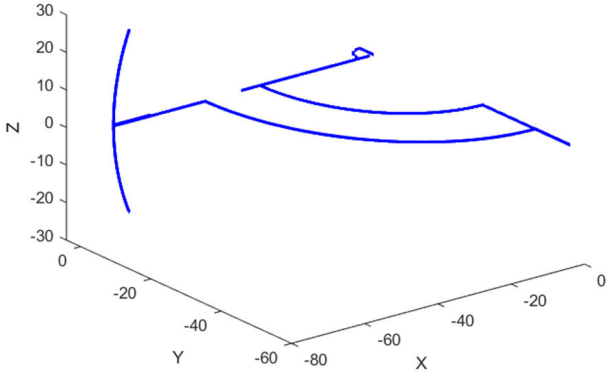

FIGURE 4. Reference trajectory.

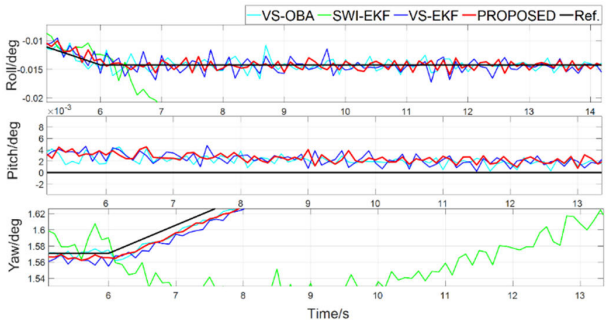

FIGURE 5. Simulation attitude estimate by different method.

Kalman filter, and the algorithm compensates for the attitude error at the initial moment, rather than the online estimation and compensation of the attitude error at the current moment, resulting in attitude divergence, which is the same as The theory of insufficient extended Kalman filtering presented in Section III-A is consistent. However, the algorithm proposed in this paper converges to the small angle of the three attitude angles, and there is no divergence because the algorithm proposed in this paper is the same as the FIMA algorithm, which is to compensate for the attitude error of the *b* system,

TABLE 3. IMU parameters.

Parameter	Specification
Gyro In-run Bias Stability	$2\ ^{o}/h$
Gyro Angle Random Walk	$0.15\ ^{o}/\sqrt{h}$
Acc. In-run Bias Stability	3.6 ug
Acc. Velocity Random Walk	$0.12\ m/s/\sqrt{h}$
IMU Refresh Rate	200 HZ
GPS Refresh Rate	1 Hz

TABLE 4. SINS system initial state.

Parameter	Specification
Initial Latitude and Longitude Height	$[114.472 \quad 30.460]_{\circ}$
Initial Posture Angle	$[0 \quad 0 \quad 0]_{\circ}$
Initial Velocity	$[0 \quad 0 \quad 0]$ m/s

rather than the *n* system, so that there is no deficiency of the assumption that the misalignment angle of the *n* system is small, and the algorithm proposed in this paper considers the influence of gyroscope error on $\boldsymbol{C}_{b(t_{k+1})}^{b(0)}$, so as to increase the robustness of the algorithm and there is no attitude jump.

V. SPORTS CAR EXPERIMENTS

A. EXPERIMENTAL PREPARATION

In order to further prove the feasibility of the algorithm, the actual on-board measurement experiment is used to verify the effectiveness of the improved OBA algorithm. The experimental equipment is a 6-degree-of-freedom MEMS-IMU-ADIS16465, which collects data from accelerometers and gyroscopes for algorithm verification, and then carries high-precision GNSS equipment, and uses its output values as reference values for comparison. The GNSS mast arm is -0.073m (front), 0.302m (right), 0.087m (bottom). The average speed of the vehicle is about 30 km/h and the travel time is 1600 seconds. The IMU parameters are shown in Table 3, the initial state of the SINS system is shown in Table 4, and the initial reference attitude, velocity, and motion trajectory are shown in Figure 6-8 (the data sources for this experiment are all provided by the Multi-source Intelligent Navigation Laboratory of Wuhan University).

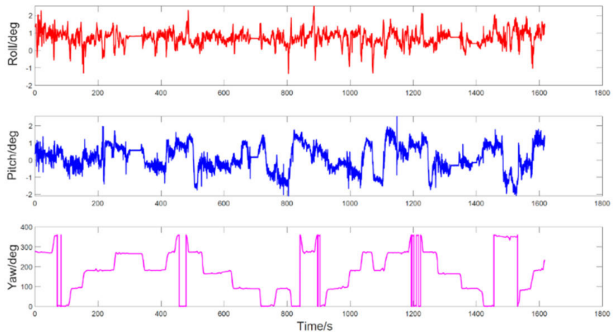

FIGURE 6. SINS system reference attitude.

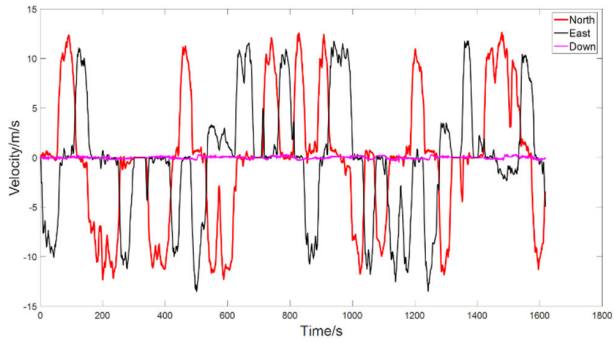

FIGURE 7. SINS system reference speed.

FIGURE 8. Automobile trajectory.

B. EXPERIMENTAL RESULTS AND ANALYSIS

To verify the effectiveness of the Kalman filter model proposed in this paper in compensating for the attitude error caused by gyroscope error, and considering the problem of accumulation of upper accelerometer error over time, the sliding window integral and vector subtraction methods are used to construct the vector for the comparative analysis of the attitude error, and the OBA algorithm, the sliding window integral + FIMA algorithm, the vector subtraction + FIMA algorithm and the Kalman filter proposed in this paper are used to filter the estimation and compensate the attitude error. Figure 9-12 shows the comparison chart of pose estimation and attitude error obtained by the four algorithms.

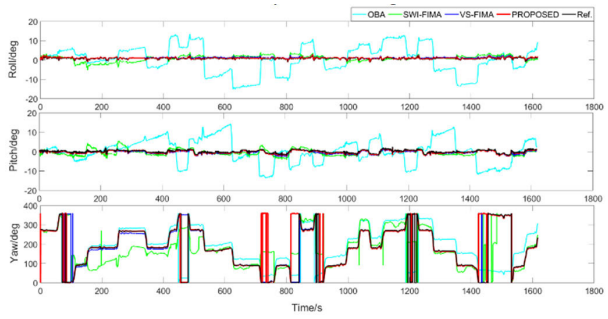

FIGURE 9. Attitude estimate by different methods.

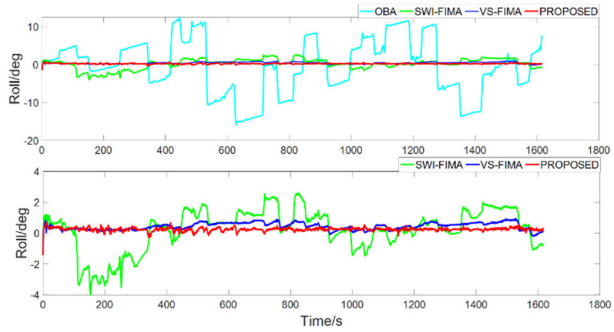

FIGURE 10. Roll estimate errors by different methods.

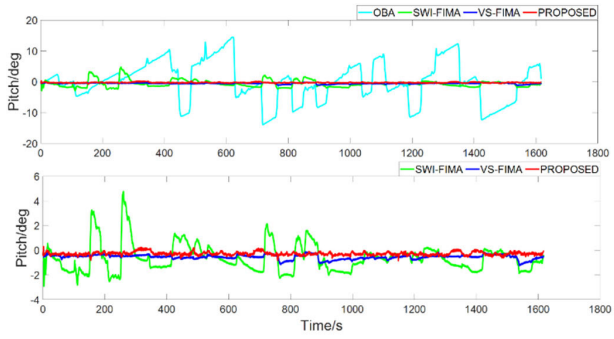

FIGURE 11. Pitch estimate errors by different methods.

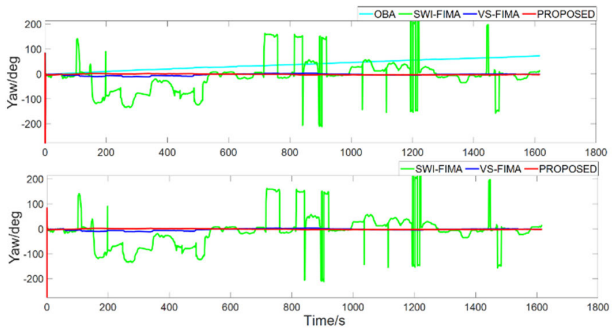

FIGURE 12. Yaw estimate errors by different methods.

To more intuitively show the different attitude accuracies of the four algorithms in the initial alignment, the attitude error results of the four algorithms are shown in Table 5 in the form of MEAN, STD, and MAX respectively.

TABLE 5. Statistics of the attitude errors.

Method	Attitude angle	Mean	Max	Std
OBA	roll	-0.3851	12.523	7.171
	pitch	0.0868	14.518	6.461
	yaw	37.6527	73.232	20.941
SWI-FIMA	roll	0.2297	-4.013	1.325
	pitch	-0.6292	4.768	1.117
	yaw	-7.4406	-276.515	67.046
VS-FIMA	roll	0.4422	0.939	0.222
	pitch	-0.5423	-1.240	0.180
	yaw	-2.9212	-12.005	3.726
PROPOSED	roll	0.2420	0.689	0.098
	pitch	-0.2701	0.245	0.135
	yaw	-1.6504	2.015	1.722

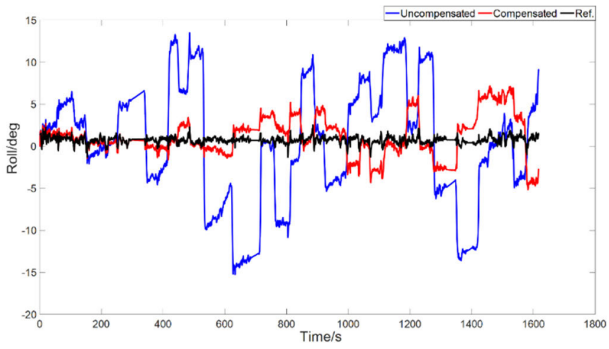

FIGURE 13. Comparison of roll angle errors of purely inertial guidance algorithms.

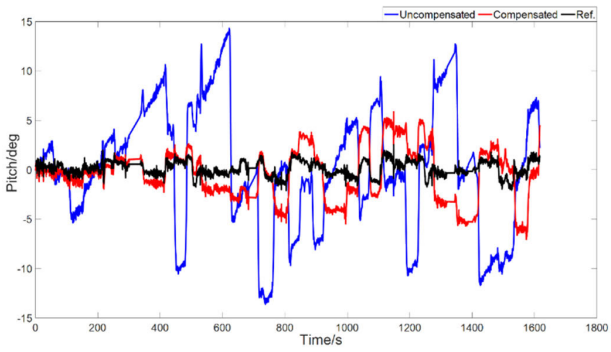

FIGURE 14. Comparison of pitch angle errors of purely inertial guidance algorithms.

As can be seen from Figure 9-12, the FIMA algorithm can achieve low-cost INS initial alignment by combining sliding window integration or vector subtraction, but the stability of initial alignment combined with vector subtraction is not as good as that combined with sliding window integration. Although the stability of the sliding window integral is improved, there is still a small jump change, which is mainly because the matrix $\boldsymbol{C}_{b(t_{k+1})}^{b(0)}$ of the FIMA algorithm does not consider the influence of gyroscope error, so that the algorithm may not be able to compensate for the attitude error well, resulting in the jump of the attitude angle. The algorithm proposed in this paper is the most stable among the five algorithms, and there is no jump change in the three attitude angles, because the proposed algorithm considers the influence of gyroscope error, compensates for the attitude error of the matrix $\boldsymbol{C}_{b(t_k)}^{b(0)}$, and feeds back the result into the construction of multiple vectors. The algorithm proposed in this paper is different from the extended Kalman filter, and there is no assumption that the misalignment angle is destroyed, because the algorithm selects the equivalent rotation vector between the b system and the b' system, and there is no gyroscope error accumulation over time before the system starts to run, so there is no misalignment angle between the b system and the b' system, and then the algorithm performs real-time attitude estimation and compensation, so the B system misalignment angle always satisfies the assumption that the b system is a small angle, so there will be no initial alignment failure.

Table 5 shows the attitude error information of the four algorithms. The OBA algorithm and the SWI-FIMA algorithm have poor accuracy due to the initial alignment failure, and the three attitude angles of the OBA algorithm belong to the divergent state, and the convergence effect of the SWI-FIMA algorithm on the roll angle and pitch angle is stronger than that of the traditional OBA algorithm, but the attitude estimation effect of the heading angle is very poor, and the standard deviation of the two algorithms is also the largest among the four algorithms, which shows that the three attitude angles obtained by the two algorithms have a high degree of dispersion and the algorithm is not robust, which is also reflected in Figure 9-12. Compared with the SWI-FIMA algorithm, the VS-FIMA algorithm has improved accuracy, reduced standard deviation, and decreased dispersion, but because the matrix $\boldsymbol{C}_{b(t_{k+1})}^{b(0)}$ does not consider the influence of gyroscope error, there is still a certain discreteness, especially the standard deviation of the heading angle reaches 3.726°. The mean, standard deviation, and maximum values of the three attitude angles of the proposed algorithm are the minimum among the five algorithms, indicating that the algorithm has the highest robustness and the lowest degree of dispersion of the three attitudes, which is the best among the four algorithms.

To verify the effectiveness of the gyroscope bias estimation of the proposed algorithm, the estimated gyroscope bias is written into the pure inertial navigation algorithm for compensation, and the effect of compensation is shown in Figs. 13 to Fig. 15.

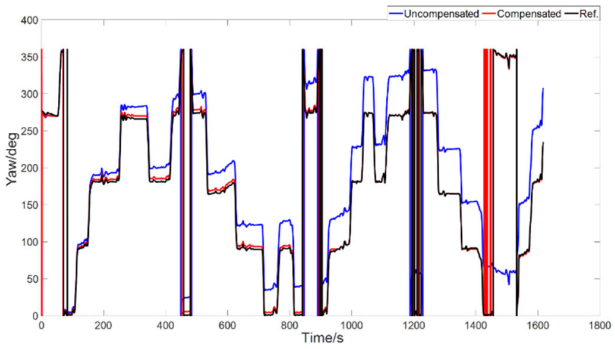

FIGURE 15. Comparison of yaw angle errors of purely inertial guidance algorithms.

As can be seen in Figure 13-15, the three attitude errors of the pure inertial navigation algorithm after gyroscope bias compensation are significantly smaller than the effect before compensation, indicating that the algorithm proposed in this paper is effective for gyroscope bias estimation. The main reason for the attitude error after compensating for gyroscope bias is that it is impossible to completely compensate the IMU's bias in practice, and it can only be compensated as much as possible to make the bias as small as possible, and the output of the IMU also contains random errors, and over time, the error of the IMU will accumulate more and more, so the essence of inertial navigation is that it will diverge, but the difference between fast and slow divergence. The pure inertial navigation algorithm does not make feedback corrections for the three attitude errors, and even small gyroscope errors and accelerometer errors can accumulate over time.

VI. CONCLUSION

A new initial alignment scheme for a GNSS-assisted low-cost INS integrated navigation system in the scenario of moving base (such as vehicle and aircraft motion alignment) has been designed and analyzed in this paper. Its feasibility has been verified through formula theory, simulation experiments, and vehicle measurement experiments. The main work and significance of this article are as follows:

1. To solve the problem of accelerometer error accumulation over time, a vector subtraction method is proposed instead of sliding window integral to construct vectors. This reduces the amount of computation, improves computational efficiency, and suppresses the accumulation of accelerometer errors over time. The algorithm also uses the least squares optimal estimation theory to solve the continuous attitude based on the constructed velocity vector.

2. To overcome the influence of gyroscope error accumulation over time, a new Kalman filter model was proposed. The equation of state and the measurement equation were reconstructed. The velocity and position information of GNSS was used as the observation and measurement, and the three attitude information of the IMU and the gyroscope bias were the state quantities. The designed Kalman filter was used to identify the three attitude misalignment angles of the load system and the gyroscope bias, and fed back to the vector construction process, to suppress the accumulation of gyroscope errors over time. The proposed Kalman filter does not have the defect that the extended Kalman filter may be destroyed by the assumption of small angles, nor does it have a matrix that ignores the influence of gyroscope error.

3. Finally, the feasibility of the proposed method is verified by simulation, and the performance of the algorithm is verified by vehicle measurement experiments. Simulation experiments verify the feasibility of the proposed method. The experimental results show that the vector subtraction construction vector proposed in this paper effectively improves the computational efficiency and reduces the computational complexity of the algorithm. The Kalman filter model proposed in this paper accurately estimates and compensates for attitude errors of the load system. The heading angle of the algorithm converges to less than 2° within 2s, and the heading angle accuracy is also maintained stably in the future.

In summary, the algorithm proposed in this paper can complete the initial alignment task under the condition of GNSS-assisted low-cost INS integrated navigation moving base, which has certain engineering practical value.

REFERENCES

[1] S. Li, "Research on in-motion alignment technology of low-cost MEMS-INS/GNSS," M.S. thesis, Wuhan Univ., Wuhan, China, 2018.

[2] Q. Fu, S. Li, Y. Liu, and F. Wu, "Information-reusing alignment technology for rotating inertial navigation system," *Aerosp. Sci. Technol.*, vol. 99, Apr. 2020, Art. no. 105747, doi: 10.1016/j.ast.2020.105747.

[3] Y.-F. Liang, P.-F. Jiang, J.-N. Xu, W. An, and M. Wu, "Initial alignment of compass based on genetic algorithm-particle swarm optimization," *Defence Technol.*, vol. 16, no. 1, pp. 257–262, Feb. 2020, doi: 10.1016/j.dt.2019.08.001.

[4] L. Li, H. Yulong, C. Lubin, and Z. Yonggang, "Development and prospects of initial alignment method for strap-down inertial navigation system," *Chin. J. Ship Res.*, vol. 17, no. 5, pp. 301–313, 2022, doi: 10.19693/j.issn.1673-3185.02884.

[5] T. Du, L. Guo, and J. Yang, "A fast initial alignment for SINS based on disturbance observer and Kalman filter," *Trans. Inst. Meas. Control*, vol. 38, no. 10, pp. 1261–1269, Oct. 2016.

[6] H. Xing, Z. Chen, H. Yang, C. Wang, Z. Lin, and M. Guo, "Self-alignment MEMS IMU method based on the rotation modulation technique on a swing base," *Sensors*, vol. 18, no. 4, p. 1178, Apr. 2018, doi: 10.3390/s18041178.

[7] F. Yu, "Research on starpdown compasslignment in dynamic environment based on forward and reverse navigation solution," M.S. thesis, Harbin Inst. Technol., Harbin, China, 2019.

[8] L. Gao, "Attitude estimation of rotating ammunition based on geomagnetic/MEMS gyro information fusion," M.S. thesis, North Univ. China, Taiyuan, China, 2021.

[9] E. H. Shin and N. EI. Sheimy, "Accuracy improvement of low-cost INS/GPS for land applications," in *Proc. Nat. Tech. Meeting Inst. Navigat.*, Jan. 2002, pp. 146–157.

[10] P. D. Groves, *Principles of GNSS, Inertial, and Multi-sensor Integrated Navigation Systems*. Norwood, MA, USA: Artech House, 2008, pp. 577–580.

[11] M. Wu, Y. Wu, X. Hu, and D. Hu, "Optimization-based alignment for inertial navigation systems: Theory and algorithm," *Aerosp. Sci. Technol.*, vol. 15, no. 1, pp. 1–17, Jan. 2011, doi: 10.1016/j.ast.2010.05.004.

[12] Y. Wu and X. Pan, "Velocity/position integration formula—Part I: Application to in-flight coarse alignment," *IEEE Trans. Aerosp. Electron. Syst.*, vol. 49, no. 2, pp. 1006–1023, Apr. 2013, doi: 10.1109/TAES.2013.6494395.

[13] Y. Wu and X. Pan, "Velocity/position integration formula—Part II: Application to strapdown inertial navigation computation," *IEEE Trans. Aerosp. Electron. Syst.*, vol. 49, no. 2, pp. 1024–1034, Apr. 2013, doi: 10.1109/TAES.2013.6494396.
[14] Q. Zhang, S. Li, Z. Xu, and X. Niu, "Velocity-based optimization-based alignment (VBOBA) of low-end MEMS IMU/GNSS for low dynamic applications," *IEEE Sensors J.*, vol. 20, no. 10, pp. 5527–5539, May 2020, doi: 10.1109/JSEN.2020.2970277.
[15] X. Xu, D. Xu, T. Zhang, and H. Zhao, "In-motion coarse alignment method for SINS/GPS using position loci," *IEEE Sensors J.*, vol. 19, no. 10, pp. 3930–3938, May 2019, doi: 10.1109/JSEN.2019.2896274.
[16] Y. Yao, X. Xu, T. Zhang, and G. Hu, "An improved initial alignment method for SINS/GPS integration with vectors subtraction," *IEEE Sensors J.*, vol. 21, no. 16, pp. 18256–18262, Aug. 2021, doi: 10.1109/JSEN.2021.3085742.
[17] Y. Huang, Y. Zhang, and X. Wang, "Kalman-filtering-based in-motion coarse alignment for odometer-aided SINS," *IEEE Trans. Instrum. Meas.*, vol. 66, no. 12, pp. 3364–3377, Dec. 2017, doi: 10.1109/TIM.2017.2737840.
[18] L. Chang, J. Li, and S. Chen, "Initial alignment by attitude estimation for strapdown inertial navigation systems," *IEEE Trans. Instrum. Meas.*, vol. 64, no. 3, pp. 784–794, Mar. 2015, doi: 10.1109/TIM.2014.2355652.
[19] L. Chang, B. Hu, and Y. Li, "Backtracking integration for fast attitude determination-based initial alignment," *IEEE Trans. Instrum. Meas.*, vol. 64, no. 3, pp. 795–803, Mar. 2015, doi: 10.1109/TIM.2014.2359516.
[20] L. Chang, F. Qin, and A. Li, "A novel backtracking scheme for attitude determination-based initial alignment," *IEEE Trans. Autom. Sci. Eng.*, vol. 12, no. 1, pp. 384–390, Jan. 2015, doi: 10.1109/TASE.2014.2346581.
[21] L. Chang, F. Zha, and F. Qin, "Indirect Kalman filtering based attitude estimation for low-cost attitude and heading reference systems," *IEEE/ASME Trans. Mechatronics*, vol. 22, no. 4, pp. 1850–1858, Aug. 2017, doi: 10.1109/TMECH.2017.2698639.
[22] Z. Lu, J. Li, X. Zhang, K. Feng, X. Wei, D. Zhang, J. Mi, and Y. Liu, "A new in-flight alignment method with an application to the low-cost SINS/GPS integrated navigation system," *Sensors*, vol. 20, no. 2, p. 512, Jan. 2020, doi: 10.3390/s20020512.
[23] W. Wang, M. Liu, and B. Xue, "Fast initial alignment of GPS-assisted SINS system on moving base," *J. Harbin Inst. Technol.*, vol. 52, no. 12, pp. 49–57, 2020, doi: 10.11918/201905245.
[24] W. Liu, X. Cheng, P. Ding, and P. Cao, "An optimal indirect in-motion coarse alignment method for GNSS-aided SINS," *IEEE Sensors J.*, vol. 22, no. 8, pp. 7608–7618, Apr. 2022, doi: 10.1109/JSEN.2022.3153093.
[25] Y. Chen, W. Li, and Y. Wang, "A robust adaptive indirect in-motion coarse alignment method for GPS/SINS integrated navigation system," *Measurement*, vol. 172, Feb. 2021, Art. no. 108834, doi: 10.1016/j.measurement.2020.108834.
[26] Y. Huang, Y. Zhang, and L. Chang, "A new fast in-motion coarse alignment method for GPS-aided low-cost SINS," *IEEE/ASME Trans. Mechatronics*, vol. 23, no. 3, pp. 1303–1313, Jun. 2018, doi: 10.1109/TMECH.2018.2835486.
[27] J. Li, J. Xu, L. Chang, and F. Zha, "An improved optimal method for initial alignment," *J. Navigat.*, vol. 67, no. 4, pp. 727–736, Jul. 2014, doi: 10.1017/s0373463314000198.
[28] L. Chang, H. He, and F. Qin, "In-motion initial alignment for odometer-aided strapdown inertial navigation system based on attitude estimation," *IEEE Sensors J.*, vol. 17, no. 3, pp. 766–773, Feb. 2017, doi: 10.1109/JSEN.2016.2633428.
[29] P. M. G. Silson, "Coarse alignment of a ship's strapdown inertial attitude reference system using velocity loci," *IEEE Trans. Instrum. Meas.*, vol. 60, no. 6, pp. 1930–1941, Jun. 2011, doi: 10.1109/TIM.2011.2113131.
[30] K. Taizhong, F. Jiancheng, and W. Wei, "In-flight calibration approach based on quaternion optimization for POS used in airborne remote sensing," *IEEE Trans. Instrum. Meas.*, vol. 62, no. 11, pp. 2882–2889, Nov. 2013, doi: 10.1109/TIM.2013.2258243.
[31] L. Ma, K. Wang, and M. Shao, "Initial alignment on moving base using GPS measurements to construct new vectors," *Measurement*, vol. 46, no. 8, pp. 2405–2410, Oct. 2013, doi: 10.1016/j.measurement.2013.04.058.
[32] D. Z. Zheng, *Linear System Theory*. Beijing, China: Tsinghua Univ. Press, May 2005.

MENGBO SUN received the B.E. degree in geographic information science from Nanning Institute of Technology, China, in 2022. She is currently pursuing the M.S. degree in resources and environment with Guilin University of Technology.

Her main research interests include the initial alignment of inertial navigation and the application and research of integrated navigation technology.

JIAN HUANG received the M.E. degree.

He is currently a Senior Engineer and the Director of Guangxi Natural Resources Product Quality Inspection Centre. He has long been engaged in the construction of natural resources quality systems and quality control of natural resources data results. He holds certificates of copyright for computer software, including "Field Verification System for Land Remediation Review Results," "Map Technology Review System," "Quality Inspection System for Guangxi Natural Resources Confirmation and Real Estate Registration Results," "Integrated System of Field and Office Based on Real-time Positioning for Topographic Maps," and "Data Collection and Evaluation System for Topographic Maps Based on Real-Time Positioning." He led the research and development projects, such as "Research and Development of Digital Level Instrument Calibration Collection and Processing System" project and the "Metrological Verification Procedures for Level Ruler Calibration Devices" project.

Mr. Huang was awarded the 2022 Guangxi Surveying and Mapping Geographic Information Science and Technology Award and the Bayu Artificial Intelligence Science and Technology Award.

PENGCHENG HU received the B.E. degree in computer science and technology from Chongqing Jiaotong University, China, in 2020. He is currently pursuing the master's degree in surveying and mapping science and technology with Guilin University of Technology, China.

He has authored or coauthored several papers on image processing, photogrammetric data processing, and other research areas. His main research interests include computer vision, image fusion, and photogrammetry data processing and applications.

XIAOHUI SONG received the B.E. degree in surveying and mapping engineering from Xiamen Institute of Technology, China, in 2021. He is currently pursuing the master's degree in resources and environment with Guilin University of Technology.

His main research interests include UAV data processing and applications.

ZHU LI (Member, IEEE) received the B.E. degree in civil engineering from Nanyang Normal University, in 2019. He is currently pursuing the master's degree in surveying and mapping science and technology with Guilin University of Technology, China.

His main research interest includes GNSS data processing.